HHS Public Access

Author manuscript

*J Am Acad Orthop Surg*. Author manuscript; available in PMC 2018 July 23.

Published in final edited form as:

*J Am Acad Orthop Surg*. 2017 February ; 25(Suppl 1): S7–S12. doi:10.5435/JAAOS-D-16-00630.

# Preclinical evaluation of photoacoustic imaging as a novel noninvasive approach to detect an orthopaedic implant infection

**Yu Wang, PhD**, **John M. Thompson, MD**, **Alyssa G. Ashbaugh, BA**, **Pavlo Khodakivskyi, PhD**, **Ghyslain Budin, PhD**, **Riccardo Sinisi, PhD**, **Andrew Heinmiller, MS**, **Marleen van Oosten, MD**, **Jan Maarten van Dijl, PhD**, **Gooitzen M van Dam, MD, PhD**, **Kevin P. Francis, PhD**, **Nicholas M. Bernthal, MD**, **Elena A. Dubikovskaya, PhD**, and **Lloyd S. Miller, MD, PhD**

## Abstract

**Introduction—**Diagnosing prosthetic joint infection (PJI) poses significant challenges, and current modalities are fraught with low sensitivity and/or potential morbidity. Photoacoustic imaging (PAI) is a novel ultrasound-based modality with potential for diagnosing PJI safely and noninvasively.

**Materials—**In an established preclinical mouse model of bioluminescent *Staphylococcus aureus* PJI, fluorescent indocyanine green (ICG) was conjugated to β-cyclodextrin (CDX-ICG) or teicoplanin (Teic-ICG) and injected intravenously 1-week postoperatively. Daily fluorescent imaging (FLI) and PAI were used to localize and quantify tracer signals. Results were analyzed with 2-way ANOVA.

**Results—**Fluorescence clearly localized to the site of infection and was significantly higher with Teic-ICG compared to CDX-ICG ($P$=0.046) and ICG-alone ($P$=0.0087). With PAI, the photoacoustic signal per volumetric analysis was substantially higher and better visualized with Teic-ICG compared to CDX-ICG and ICG-alone, and co-localized well with BLI /FLI.

**Conclusion—**Photoacoustic imaging can successfully localize PJI in this proof-of-concept study and has shown potential for clinical translation in orthopaedics.

## INTRODUCTION

Diagnosing prosthetic joint infection (PJI) remains a challenging clinical dilemma, as noninvasive modalities have low sensitivity and invasive ones carry potential associated morbidity. Oftentimes signs and symptoms of PJI such as edema, pain, and erythema are equivocal or even absent. The current clinical algorithm for diagnosing PJI includes pertinent history, detailed physical exam, and obtaining laboratory inflammatory markers such as C-reactive protein (CRP) and erythrocyte sedimentation rate (ESR) [1]. When the index of suspicion is sufficiently high, invasive testing such as joint aspiration for Gram stain and culture may be confirmatory. Per the American Association of Orthopaedic Surgeons (AAOS) clinical practice guidelines[2], a definitive diagnosis is made when 1 major (draining sinus tract or 2 positive joint aspirations) or 4 minor criteria (a single positive aspiration

Correspondence to: David C. Smith, BA, American Academy of Orthopaedic Surgeons, Publications, 9400 W Higgins Rd, Rosemont, IL 60018, UNITED STATES, 847-384-4122, smith@aaos.org.

culture, elevated ESR/CRP, elevated synovial white blood cell [WBC] count or neutrophil percentage, gross purulence at the time of surgery, or >5 neutrophils in high-powered field on frozen section) are present.

While these guidelines have standardized and improved diagnosis of PJI, both major and minor criteria unfortunately by definition require invasive testing to obtain a fluid or tissue sample. Joint aspiration is a relatively benign procedure but may potentially introduce infection into an otherwise sterile joint, inadvertently damage cartilage or neurovascular structures, or cause vasovagal reactions placing the patient at risk for harm[3]. Furthermore, diagnosis of PJI per these criteria based on current technologies may not be possible preoperatively, which may interfere with surgical planning and timely treatment and place patients at risk for perioperative complications.

Noninvasive imaging technologies are particularly attractive for diagnosing PJI as they avoid potential contamination of the joint and discomfort for the patient. Ultrasound (US) imaging modalities have gained traction in numerous fields of medicine due to noninvasiveness, versatility, depth of tissue penetration, and safety for the patient. For example, Focused Abdominal Series for Trauma (FAST) has revolutionized the manner in which abdominal trauma is safely and noninvasively identified and rapidly screened for possible operative intervention[4]. Within orthopaedics, ultrasound has already been successfully used to aid diagnosis of upper extremity abscesses[5, 6] as well as identify rotator cuff tears[7, 8].

A novel imaging modality based on US is photoacoustic imaging (PAI). In essence, laser pulses are directed into the body at a specific wavelength to excite a photoacoustic tracer attached to the target tissue. In turn, the tracer heats and undergoes thermo-elastic expansion, thus releasing ultrasonic pressure waves that can then be detected by the photoacoustic receiver[9]. This two-dimensional information can then be reconstructed into a three-dimensional representation of the underlying tissue and associated signal[10]. PAI provides tissue detail comparable to that of conventional MRI and can operate at a depth of up to 8 cm[11, 9], making it an attractive imaging modality for clinical applicability.

Bioluminescence (BLI) and fluorescence imaging (FLI) provide an ideal preclinical technology for studying PJI in translational settings[12, 13] but remain limited in their direct clinical application due to suboptimal depth of penetration stemming from the epi-illumination characteristics[14]. Although near-infrared fluorescent dyes have greater tissue penetration depths (3–5 cm) compared to BLI (1–2 cm)[14], photoaocustic imaging provides significant deeper tissue penetration. Bioluminescent bacteria allow for monitoring disease burden (i.e. bacterial growth) while fluorescent tracers can be used to highlight target tissue[15]. Currently, there is no described role for PAI imaging in orthopaedics. We hypothesized that novel fluorescent tracers of infection consisting of indocyanine green (ICG) conjugated to β-cyclodextrin (CDX-ICG), a polysugar that is taken up by bacteria but not host cells, or conjugated to teicoplanin (Teic-ICG), an antibiotic that targets cell wall synthesis of Gram-positive bacteria, would localize to the site of a *Staphylococcus aureus* infection in a mouse model of PJI and provide proof-of-concept for detecting PJI noninvasively with PAI.

## MATERIALS AND METHODS

### Synthesis

6-Monodeoxy-6-monoamino-β-cyclodextrin hydrochloride (Cyclodextrin-Shop, Tilburg, the Netherlands), ICG-NHS ester (Intrace Medical, Lausanne, Switzerland), ICG and teicoplanin (mixture of teicoplanins $A_2$, 80%+, Sigma-Aldrich) were used as purchased. Analytical HPLC was performed on a Waters ACQUITY UPLC Class H instrument using BEH C18 1.7 um 2.1×50 mm column with a gradient over 4 min of 5% to 100% acetonitrile in water containing 0.1% formic acid, and preparative HPLC was performed on a Waters HPLC system using XTerra Prep Ms C18 OBD 5 um 19×50 mm column with a gradient over 10 min of 5% to 100% acetonitrile in water containing 0.1% formic acid.

### CDX-ICG conjugate

To a solution of ICG-NHS ester (10 mg, 0.012 mmol) in dry DMSO (2 mL) were added 6-monodeoxy-6-monoamino-β-cyclodextrin hydrochloride (16.4 mg, 0.014 mmol) and DIPEA (10.4 uL, 0.060 mmol) with stirring in a light-protected flask. The reaction mixture was stirred for 3 hours at ambient temperature and purified using preparative HPLC to give 9.4 mg (42 %) of title product as a green solid. ESI-QTOF-MS: m/z calc. for $[M+2H]^{2+}$ 923.3596, found 923.3592.

### Teic-ICG conjugate

To a solution of ICG-NHS ester (20.1 mg, 0.022 mmol) in dry DMSO (2 mL) were added teicoplanin (50.0 mg, 0.027 mmol) and DIPEA (19.0 uL, 0.111 mmol) with stirring in a light-protected flask. The reaction mixture was stirred for 3 hours at ambient temperature and purified using preparative HPLC to give 25.3 mg (36 %) of title product as a green solid. ESI-QTOF-MS: m/z calc. for $[M-H+2Na]^{+}$ 2635.8696, found 2635.8279.

### Bacteria preparation

The *S. aureus* strain Xen36 (PerkinElmer, Hopkinton, MA) used in this study was previously derived from the clinical bacteremia isolate ATCC 49525 (Wright)[16]. It possesses a stably integrated bioluminescent luciferase gene construct that is maintained in all progeny without selection, and only metabolically active bacteria emit light. Xen36 was prepared for inoculation as previously described[17]. Briefly, Xen36 was streaked onto plates containing tryptic soy broth (TSB) plus 1.5% Bacto agar (Becton, Dickinson, Sparks, MD). Colonies of Xen36 were grown overnight at 37°C in a shaking incubator (240 rpm) in TSB. Mid-logarithmic-phase bacteria were obtained after a 2-h subculture of a 1:50 dilution of the overnight culture.

### Mice

10-week-old male C57BL/6 mice obtained from Jackson Laboratories (Bar Harbor, ME) were used in all experiments.

### Mouse surgical procedures

All procedures were approved by the Johns Hopkins University Animal Care and Use Committee (protocol # M015M421). This surgical mouse model of PJI was performed as previously described[17]. Briefly, a medical-grade titanium Kirschner wire (K-wire) (0.6 mm×9mm) (Modern Grinding, Port Washington, WI) was surgically placed into the femur in a retrograde fashion with 1 mm protruding into the joint space. Xen36 (1000 colony formation units [CFU] in 2 μl saline) was inoculated onto the protruding implant using a micropipette. The patella was relocated, and the surgical site was closed with absorbable sutures. Sustained-release buprenorphine (2.5 mg/kg) (ZooPharm, WY) was administered subcutaneously at the time of surgery.

### Fluorescent tracer administration

On day 7 post-infection, two mice each were injected with ICG alone (negative control), CDX-ICG, or Teic-ICG through the retro-orbital vein (2.5 mM/kg).

### *In vivo* bioluminescent and fluorescent imaging

To noninvasively measure the bacterial burden and the fluorescent signal, *in vivo* bioluminescent and fluorescent imaging were performed using the IVIS Lumina III imaging system (PerkinElmer, Hopkinton, MA) on day 1, 2, 3, and 4 after fluorescent tracer administration. Bioluminescence was measured for 5min via maximum flux (p/s) while fluorescence was measured over 0.5s with excitation and emission wavelengths of 780 nm and 845 nm, respectively, via maximum radiant efficiency ([p/s]/[μW/cm$^2$]).

### Photoacoustic Imaging

Ultrasound and photoacoustic imaging were performed using the Vevo LAZR photoacoustic and microultrasound imaging system (FUJIFILM VisualSonics, Toronto, Canada) using the LZ-250 transducer which has a center frequency of 21 MHz. A 3D stepper motor moved the probe during image acquisition to collect a 3D data set. Multispectral photoacoustic imaging was performed using Nanostepper mode whereby each slice of the 3D scan consisted of images taken at 680, 730, 750, 800, 850 and 900 nm wavelengths. In addition, a Spectro mode acquisition was performed at a single slice where images were taken between 680 and 970 nm in 5 nm increments. For post-processing, wavelength subtraction was used to isolate signal from the ICG-based dye from the background hemoglobin signal. Images were rendered using the VevoLAB software (FUJIFILM VisualSonics, Toronto, Canada) and contours were drawn around structures identified in the high-frequency ultrasound images such as the femur (white), tibia (light blue), skin (dark blue) and lymph nodes (yellow) (see movie). Signal from the dye (green) as identified from the photoacoustic image was similarly contoured and all drawn regions were rendered as wireframe structures within the software. A strong photoacoustic signal at all wavelengths used from within the end of the femur was identified and similarly contoured and rendered to identify the orthopaedic implant (red). Signal was calculated as % signal within the volumetric region of interest (ROI).

### Statistical analysis

Bioluminescence and fluorescence are expressed as mean ± standard error of the mean (SEM) and were compared using 2-way ANOVA.

## RESULTS

### *In vivo* bioluminescence and fluorescence

All mice developed robust infections at the surgical site and implant by the time of fluorescent tracer injection 7 days after surgery. After administration of fluorescent tracer (day 0), BLI remained steady over time and was not significantly different between groups (Figure 1). FLI demonstrated maximum signal on day 1 for all groups with values for ICG alone, CDX-ICG, and Teic-ICG of $3.05 \pm 0.32 \times 10^8$, $4.74 \pm 0.52 \times 10^9$, and $9.17 \pm 0.54 \times 10^9$, respectively. Fluorescent signal subsequently decreased daily but was significantly higher at all time points at the surgical site/implant of mice injected with Teic-ICG ($P$=0.0087) or CDX-ICG ($P$=0.0046) compared to negative control ICG alone (Figure 1). Moreover, the fluorescent signal observed with Teic-ICG was significantly higher overall ($P$=0.046) compared to CDX-ICG.

### Photoacoustic imaging

Photoacoustic signals from the 3 fluorescent tracers were analyzed in a volumetric manner with PAI on day 4. On 3D reconstruction, the burden of infection was distinguishable from surrounding tissue and background noise in the Teic-ICG-treated group but not in the other groups (Figure 2, Movie S1). The volume of the hindlimb was measured in ICG alone, CDX-ICG, and Teic-ICG-treated mice as 1483 $mm^3$, 1289 $mm^3$, and 1215 $mm^3$, respectively. The signal percentage within the ROI was substantially higher in the Teic-ICG-treated group (2.230%) compared to the ICG alone (0.329%) and CDX-ICG-treated (0.374%) groups (Figure 2).

## DISCUSSION

PJI remains difficult to detect despite rigorous algorithms and diagnostic tests that subject patients to painful and potentially harmful invasive procedures and that also may require multiple days to obtain final results. Missed and delayed diagnoses unfortunately can be catastrophic for patients, as complications and costs from delayed care may become staggering. Early and definitive detection is paramount, with emphasis on safe and noninvasive detection strategies. Ultrasound-based modalities have emerged as powerful diagnostic tools in the clinical setting for various indications. Through the development of a hybrid technique like PAI, a novel photoaocustic modality based upon US imaging, in combination with unique photoacoustic markers of infection, we have demonstrated proof-of-concept efficacy at detecting PJI in this early feasibility study.

Developing and identifying accurate clinical diagnostic tests has become a primary focus to help avoid unnecessary surgery. In terms of hematologic values, IL-6 and procalcitonin have preliminarily demonstrated diagnostic value for PJI[18, 19] and are currently under further investigation as useful clinical parameters but nevertheless remain markers associated with

systemic inflammation. For synovial fluid markers, alpha-defensin has shown high specificity and sensitivity for PJI[20], but aspiration in general is invasive and not without complication. Polymerase chain reaction (PCR) of synovial fluid may improve sensitivity and specificity of detection but in turn is potentially concerning for high false positive rates from contamination[21] and also is invasive. Nuclear medicine studies such as $^{67}$Gallium, $^{111}$In labelled leukocyte scintigraphy, $^{99}$Tc-bone scintigraphy, and $^{18}$FDG-PET-imaging have successfully diagnosed PJI[22–26], but this technology exposes patients to substantial doses of radiation. PAI is an intriguing potential adjunctive diagnostic test for PJI because it is noninvasive, uses tracers specifically designed to target infection, provides high tissue resolution at a reasonable depth of penetration, and does not involve ionizing radiation, rendering it a repetitive harmless imaging tool.

This study is unique in that PAI has never before to our knowledge been applied to orthopaedic infections. Kothapali *et al.*[27] has previously used PAI to detect markers embedded within chicken breast as a simulation for diagnosing breast and prostate cancer. They noted high spatial resolution and adequate depth of penetration of the signal, with promising potential for clinical application. Other groups have reported successful detection of various types of breast cancers in the clinical setting[28, 29]. We believe that PAI can be extrapolated into orthopaedics for a myriad of pathologies including diagnosis of PJI. Tissue penetration and strength of signal from the imaging probe and photoacoustic tracers are two current limitations of the technology, but continued advances in the field may soon overcome these shortcomings.

One of the major weaknesses of this study, as with many pre-clinical trials, is that it was performed on small animals that may have different tissue properties associated with light and sound-based imaging modalities. However, ultrasound use is widespread in the clinical setting, and PAI has already successfully been applied in clinical oncology[28, 29]. Targeting efficiency of the fluorescent tracer to the site of infection in mice may not be representative of that in humans, as there may be different immune mechanisms involved. However, these tracers are all based on clinically-approved molecules with proven efficacy in human diseases, and other near-infrared fluorescent constructs initially tested in mice have successfully translated into clinical medicine[30], creating strong potential for clinical translation of these photoacoustic tracers. Use of a mouse model of PJI may oversimplify the pathogenesis and characteristics of PJI, but this surgical model is widely accepted in the scientific community as an appropriate representation. Finally, this study was limited by small group size, but statistical significance was achieved despite the low numbers.

In conclusion, we have demonstrated proof-of-concept that photoacoustic imaging can noninvasively localize an infection in a preclinical model of PJI. Further studies may involve larger animals to further assess depth of penetration as well as identify and compare more specific photoacoustic probes before clinical application.

## Supplementary Material

Refer to Web version on PubMed Central for supplementary material.

## References


1. Minassian AM, Osmon DR, Berendt AR. Clinical guidelines in the management of prosthetic joint infection. J Antimicrob Chemother. 2014; 69(Suppl 1):i29–35. [PubMed: 25135086]
2. Parvizi J, Zmistowski B, Berbari EF, et al. New definition for periprosthetic joint infection: from the Workgroup of the Musculoskeletal Infection Society. Clin Orthop Relat Res. 2011; 469:2992–2994. [PubMed: 21938532]
3. Fessell DP, Jacobson JA, Craig J, et al. Using sonography to reveal and aspirate joint effusions. AJR Am J Roentgenol. 2000; 174:1353–1362. [PubMed: 10789795]
4. Rothlin MA, Naf R, Amgwerd M, Candinas D, Frick T, Trentz O. Ultrasound in blunt abdominal and thoracic trauma. J Trauma. 1993; 34:488–495. [PubMed: 8487332]
5. Halim A, Shih Y, Dodds SD. The utility of ultrasound for diagnosing purulent infections of the upper extremity. Hand (N Y). 2015; 10:701–706. [PubMed: 26568726]
6. Gaspari R, Dayno M, Briones J, Blehar D. Comparison of computerized tomography and ultrasound for diagnosing soft tissue abscesses. Crit Ultrasound J. 2012; 4:5. [PubMed: 22871216]
7. Milton F, Wills AJ, Hodgson TL. The neural basis of overall similarity and single-dimension sorting. Neuroimage. 2009; 46:319–326. [PubMed: 19457383]
8. Read JW, Perko M. Shoulder ultrasound: diagnostic accuracy for impingement syndrome, rotator cuff tear, and biceps tendon pathology. J Shoulder Elbow Surg. 1998; 7:264–271. [PubMed: 9658352]
9. Ntziachristos V, Razansky D. Molecular imaging by means of multispectral optoacoustic tomography (MSOT). Chem Rev. 2010; 110:2783–2794. [PubMed: 20387910]
10. Bohndiek SE, Bodapati S, Van De Sompel D, Kothapalli SR, Gambhir SS. Development and application of stable phantoms for the evaluation of photoacoustic imaging instruments. PLoS One. 2013; 8:e75533. [PubMed: 24086557]
11. Wang LV, Hu S. Photoacoustic tomography: in vivo imaging from organelles to organs. Science. 2012; 335:1458–1462. [PubMed: 22442475]
12. Pribaz JR, Bernthal NM, Billi F, et al. Mouse model of chronic post-arthroplasty infection: noninvasive in vivo bioluminescence imaging to monitor bacterial burden for long-term study. J Orthop Res. 2012; 30:335–340. [PubMed: 21837686]
13. van Oosten M, Schafer T, Gazendam JA, et al. Real-time in vivo imaging of invasive- and biomaterial-associated bacterial infections using fluorescently labelled vancomycin. Nat Commun. 2013; 4:2584. [PubMed: 24129412]
14. van Oosten M, Hahn M, Crane LM, et al. Targeted imaging of bacterial infections: advances, hurdles and hopes. FEMS Microbiol Rev. 2015; 39:892–916. [PubMed: 26109599]
15. Niska JA, Meganck JA, Pribaz JR, et al. Monitoring bacterial burden, inflammation and bone damage longitudinally using optical and muCT imaging in an orthopaedic implant infection in mice. PLoS One. 2012; 7:e47397. [PubMed: 23082163]
16. Francis KP, Joh D, Bellinger-Kawahara C, Hawkinson MJ, Purchio TF, Contag PR. Monitoring bioluminescent Staphylococcus aureus infections in living mice using a novel luxABCDE construct. Infect Immun. 2000; 68:3594–3600. [PubMed: 10816517]
17. Bernthal NM, Stavrakis AI, Billi F, et al. A mouse model of post-arthroplasty Staphylococcus aureus joint infection to evaluate in vivo the efficacy of antimicrobial implant coatings. PLoS One. 2010; 5:e12580. [PubMed: 20830204]
18. Berbari E, Mabry T, Tsaras G, et al. Inflammatory blood laboratory levels as markers of prosthetic joint infection: a systematic review and meta-analysis. J Bone Joint Surg Am. 2010; 92:2102–2109. [PubMed: 20810860]
19. Bottner F, Wegner A, Winkelmann W, Becker K, Erren M, Gotze C. Interleukin-6, procalcitonin and TNF-alpha: markers of peri-prosthetic infection following total joint replacement. J Bone Joint Surg Br. 2007; 89:94–99. [PubMed: 17259424]
20. Deirmengian C, Kardos K, Kilmartin P, Cameron A, Schiller K, Parvizi J. Diagnosing periprosthetic joint infection: has the era of the biomarker arrived? Clin Orthop Relat Res. 2014; 472:3254–3262. [PubMed: 24590839]

21. Hartley JC, Harris KA. Molecular techniques for diagnosing prosthetic joint infections. J Antimicrob Chemother. 2014; 69(Suppl 1):i21–24. [PubMed: 25135084]
22. Glaudemans AW, Galli F, Pacilio M, Signore A. Leukocyte and bacteria imaging in prosthetic joint infection. Eur Cell Mater. 2013; 25:61–77. [PubMed: 23325539]
23. Gemmel F, Van den Wyngaert H, Love C, Welling MM, Gemmel P, Palestro CJ. Prosthetic joint infections: radionuclide state-of-the-art imaging. Eur J Nucl Med Mol Imaging. 2012; 39:892–909. [PubMed: 22361912]
24. Chryssikos T, Parvizi J, Ghanem E, Newberg A, Zhuang H, Alavi A. FDG-PET imaging can diagnose periprosthetic infection of the hip. Clin Orthop Relat Res. 2008; 466:1338–1342. [PubMed: 18421537]
25. Basu S, Kwee TC, Saboury B, et al. FDG PET for diagnosing infection in hip and knee prostheses: prospective study in 221 prostheses and subgroup comparison with combined (111)In-labeled leukocyte/(99m)Tc-sulfur colloid bone marrow imaging in 88 prostheses. Clin Nucl Med. 2014; 39:609–615. [PubMed: 24873788]
26. Levitsky KA, Hozack WJ, Balderston RA, et al. Evaluation of the painful prosthetic joint. Relative value of bone scan, sedimentation rate, and joint aspiration. J Arthroplasty. 1991; 6:237–244. [PubMed: 1940929]
27. Kothapalli SR, Ma TJ, Vaithilingam S, Oralkan O, Khuri-Yakub BT, Gambhir SS. Deep tissue photoacoustic imaging using a miniaturized 2-D capacitive micromachined ultrasonic transducer array. IEEE Trans Biomed Eng. 2012; 59:1199–1204. [PubMed: 22249594]
28. Kitai T, Torii M, Sugie T, et al. Photoacoustic mammography: initial clinical results. Breast Cancer. 2014; 21:146–153. [PubMed: 22484692]
29. Ermilov SA, Khamapirad T, Conjusteau A, et al. Laser optoacoustic imaging system for detection of breast cancer. J Biomed Opt. 2009; 14:024007. [PubMed: 19405737]
30. Weissleder R, Tung CH, Mahmood U, Bogdanov A Jr. In vivo imaging of tumors with protease-activated near-infrared fluorescent probes. Nat Biotechnol. 1999; 17:375–378. [PubMed: 10207887]

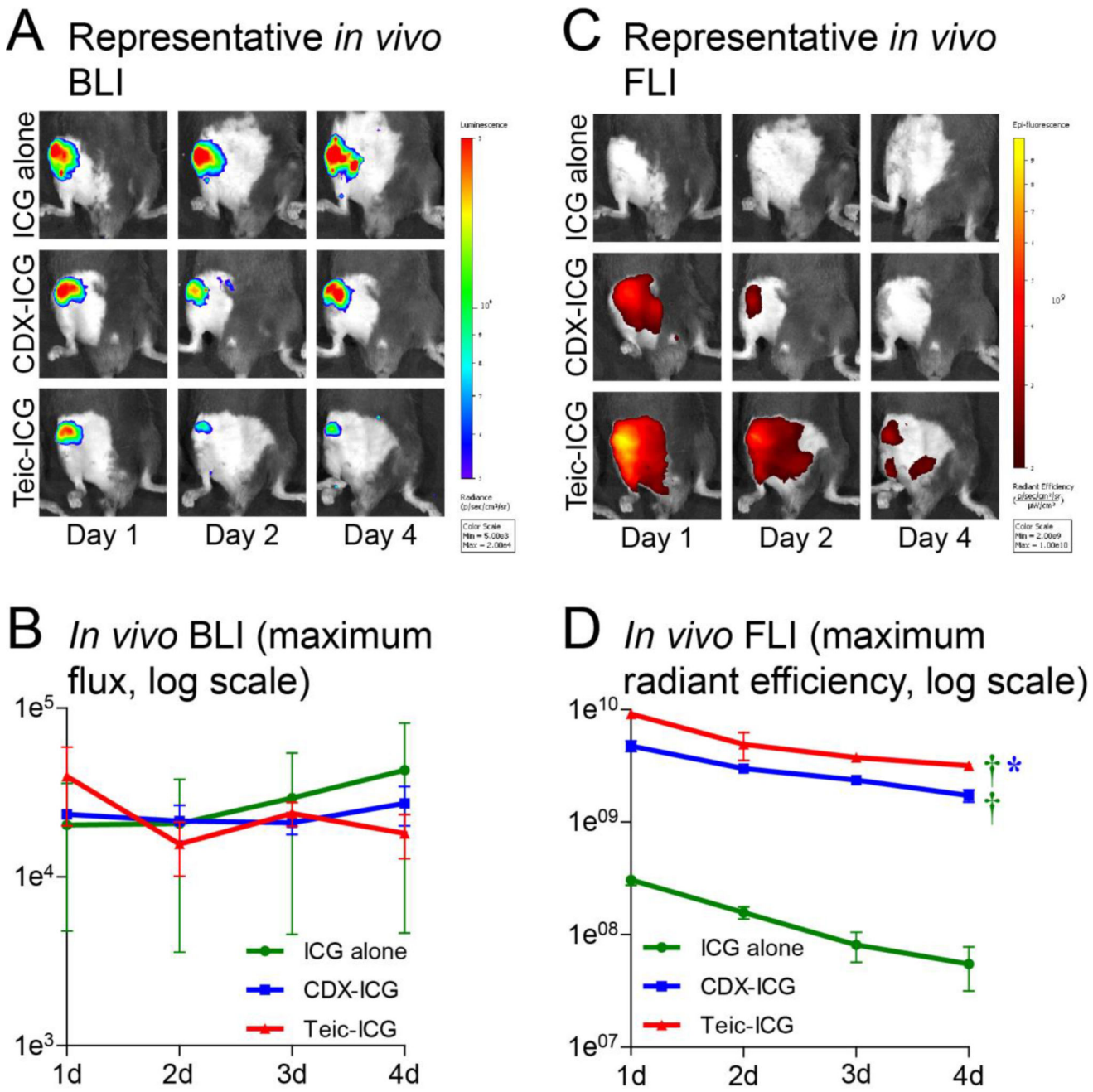


**Figure 1. In vivo bioluminescence (BLI) and fluorescence imaging (FLI)**

Mice underwent implantation of a Kirschner-wire with direct inoculation of bioluminescent *S. aureus* into the right knee. Seven days after surgery, three hybrid fluorescent / photoacoustic tracers were injected intravenously: indocyanine green (ICG) alone, or tagged to β-cyclodextrin (CDX-ICG) or teicoplanin (Teic-ICG). (A) Representative *in vivo* bioluminescence images, with signal indicative of infection localized to the surgical site. (B) Overall bioluminescence of the three tracers. No significant difference in signal was noted. (C) Representative *in vivo* fluorescence images, with localization to the surgical site in Teic-ICG and somewhat in CDX-ICG but not in ICG alone. (D) Overall fluorescence of the three

tracers. Teic-ICG ($P$=0.0087) and CDX-ICG ($P$=0.0046) were both significantly higher than ICG alone. Teic-ICG was also significantly higher than CDX-ICG ($P$=0.047).

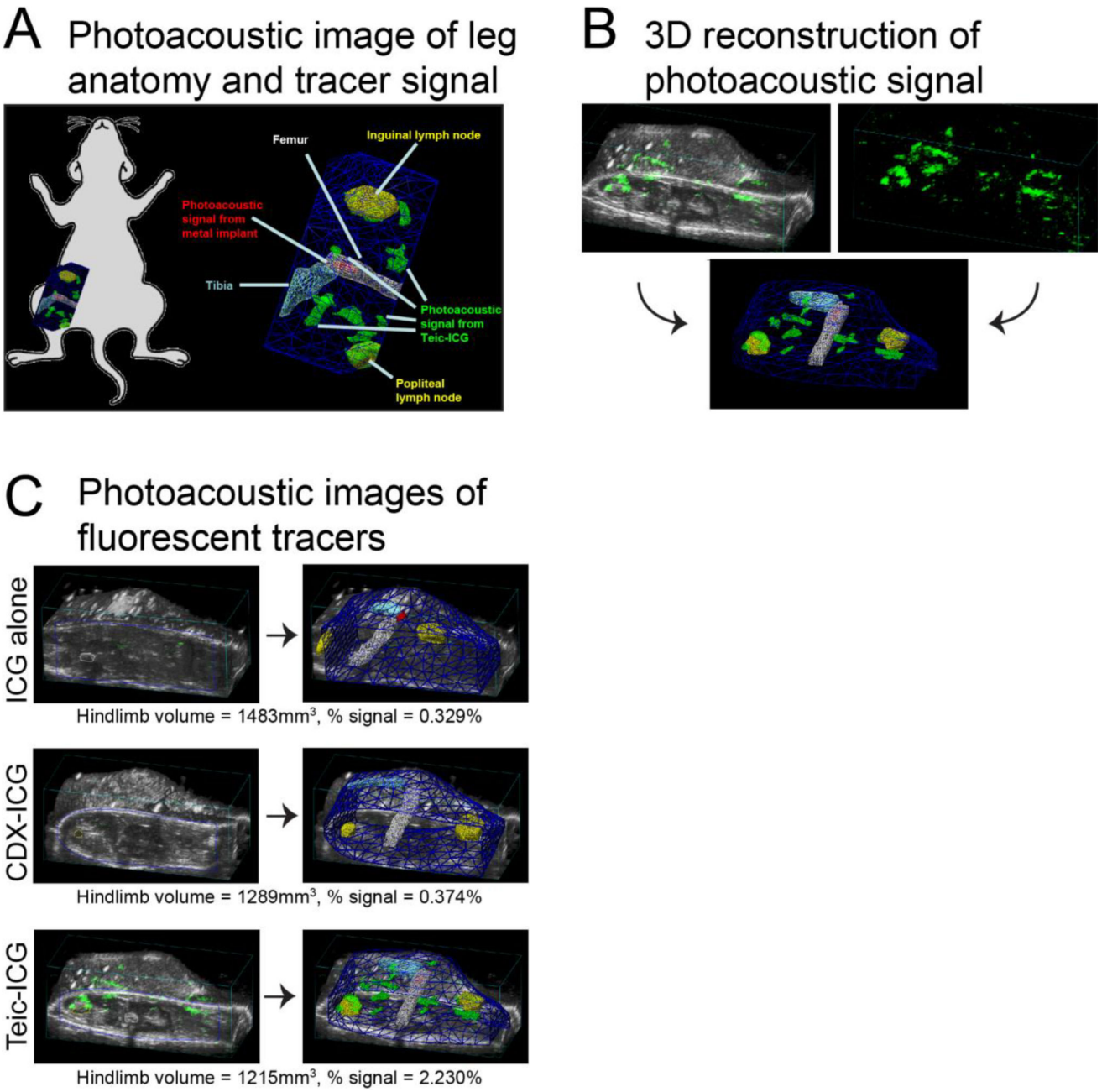


**Figure 2. Photoacoustic imaging (PAI) workflow and images**

Photoacoustic imaging was used to assess signal in the surgical hindlimb 4 days after tracer injection. (A) Graphical representation of anatomy and photoacoustic localization (green), which was detected around the implant and throughout the surgical site. (B) Representative reconstruction of two-dimensional (2D) ultrasonic and photoacoustic details (upper panels) into three-dimensional (3D) contour map (lower panel). (C) Analysis of % signal in the region of interest (ROI) on day 4 in a representative mouse from each group. Signal was substantially higher in the Teic-ICG (2.230%) compared to the ICG alone (0.329%) and the CDX-ICG-treated (0.374%) mice.